

# Corrosion and mechanical properties of plasma electrolytic oxidation-coated AZ80 magnesium alloy

Luca Pezzato<sup>1</sup>  | Leonardo Bertolucci Coelho<sup>2</sup> | Rachele Bertolini<sup>1</sup> |  
Alessio Giorgio Settimi<sup>1</sup> | Katya Brunelli<sup>1,3</sup> | Marjorie Olivier<sup>2</sup> | Manuele Dabalà<sup>1</sup>

<sup>1</sup>Department of Industrial Engineering, University of Padova, Padova, Italy

<sup>2</sup>Materials Science Department, Faculty of Engineering, University of Mons, Mons, Belgium

<sup>3</sup>Department of Civil, Environmental and Architectural Engineering, University of Padova, Padova, Italy

## Correspondence

Luca Pezzato, Department of Industrial Engineering, University of Padova, Via Marzolo 9, 35131 Padova PD, Italy.

Email: luca.pezzato@unipd.it; lucapezzato@virgilio.it

## Abstract

Plasma electrolytic oxidation (PEO) coatings were produced on AZ80 magnesium alloy in a solution containing silicates and phosphates and working at high current densities with short treatment times. The effect of a sealing treatment in boiling water on corrosion and mechanical properties of the coatings were investigated. Moreover, the corrosion mechanism of the samples with and without the sealing treatment was evaluated. The microstructure of the coatings was characterized with scanning electron microscope observation and X-ray diffraction analysis. The mechanical properties were evaluated with nanoindentation tests and the corrosion resistance was studied by potentiodynamic polarization, electrochemical impedance spectroscopy, and scanning vibrating electrode technique. The results showed that the sealing did not influence the microstructure and the mechanical properties of the samples and instead produced a remarkable increase in the corrosion resistance. The crevice corrosion, present in the sample without the sealing, was avoided with the treatment in boiling water.

## KEYWORDS

EIS, magnesium alloys, nano-hardness, PEO, sealing, SVET

## 1 | INTRODUCTION

Magnesium alloys, due to the high strain/weight ratio, have been extensively used in lightweight engineering application to improve fuel efficiency to satisfy economic and environmental transportation requirements.<sup>[1,2]</sup> However, magnesium base alloys possess poor corrosion resistance because of the high activity of Mg element.<sup>[3]</sup> To enhance the corrosion resistance, many coating techniques have been used,<sup>[4]</sup> including chemical conversion coatings,<sup>[5,6]</sup> anodizing,<sup>[7]</sup> electroplating, and electro-less plating.<sup>[8]</sup>

However, they are not adequate for use in some severe service circumstances, for example, aerospace applications. Recently, a novel promising surface treatment

method, called micro arc oxidation (MAO) or plasma electrolytic oxidation (PEO) has been developed.<sup>[9]</sup> PEO process allows the formation of durable, thick, uniform, and adherent coatings on various types of metals, including magnesium alloys, with the possibility to obtain good coatings also on components of complex shape and without subjecting the substrate to elevated temperature. Moreover, the treatment is similar to traditional anodizing and does not require highly complex equipment.<sup>[10]</sup> The characteristic of the obtained coatings depends on some important process parameters: current density, voltage, direct or pulsed current, and electrolyte composition.<sup>[11]</sup> The obtained coating resulted in richness of pores on the surface, even if an optimization of the parameters can reduce the porosity

of the coating.<sup>[12]</sup> However, generally a sealing treatment is necessary in order to ensure sufficient resistance against corrosion.<sup>[13]</sup> Different types of sealing treatments were performed in literature: with particles in order to give also particular properties to the coating,<sup>[14]</sup> with rare-earth based conversion layers,<sup>[15,16]</sup> and also with compounds that can ensure active protection.<sup>[17]</sup> However, due to the economical and practical reasons, linked also with the fact that are the ones used in traditional anodizing, the sealing treatments in boiling water remain the ones mainly used in the industrial world. The effectiveness of the sealing with boiling water was already verified for PEO coatings<sup>[13]</sup> but a systematic study on the effect of the sealing treatment on the mechanical properties and on the corrosion mechanism was not found. In this work, PEO coatings were produced on AZ80 magnesium alloy working with short treatment time and high current densities and a standard sealing treatment was performed studying the mechanism of corrosion of the sealed and unsealed samples with different electrochemical techniques. Moreover, the influence of the sealing treatment on the mechanical properties was analyzed with nanoindentation tests.

## 2 | EXPERIMENTAL PROCEDURE

### 2.1 | Sample preparation

Samples of AZ80 magnesium alloy were cut from bars and used as substrate for PEO coatings. The composition of the samples was 8.3% Al, 0.5% Zn, 0.3% Mn, 0.1% Si, Mg bal.

Before the PEO treatment, the samples were polished with standard metallographic technique (grinding with SiC abrasive papers, 500, 800, 1200, 4000, and polishing with clothes and 6–1- $\mu\text{m}$  diamond suspension) and degreased with acetone in ultrasounds.

The plasma electrolytic oxidation process was carried out using a TDK-Lambda DC power supply of 300-V/8-A capacity. During the treatment, the sample worked as anode and the cathode was the galvanized steel mesh. The electrolyte was an aqueous solution containing 40 g/L of NaOH, 50 g/L of  $\text{Na}_2\text{SiO}_3$ , and 50 g/L of  $\text{Na}_5\text{P}_3\text{O}_{10}$ . The treatments were performed maintaining the current constant and letting the potential free to vary. In detail, the current was fixed at 0.4 A/cm<sup>2</sup> and the potential grew until a plateau at 140 V. The treatment time was 3 min. The electrolyte was contained in a thermostatic bath that controlled the temperature and maintained it at 25°C. After the PEO treatment, the sealing process was performed in boiling distilled water for 30 min.<sup>[18]</sup> After the process, the samples were

washed with distilled water and ethanol and dried with compressed air. Also, untreated samples and samples without the sealing treatment were tested as comparison.

### 2.2 | Microstructural characterization

The samples were cut in the cross-section and mounted in epoxy resin and polished with standard metallographic technique, described in Section 2.1, to be observed with scanning electron microscope (SEM), in order to analyze the thickness, adhesion, and homogeneity of the coating.

The cross-sections of treated samples were examined with a Cambridge Stereoscan 440 scanning electron microscope, equipped with a Philips PV9800 EDS to also have information on the elemental composition of the coating.

The phase analysis was carried out with a Siemens D500 X-ray diffractometer using Cu  $K\alpha$  radiation.

### 2.3 | Mechanical resistance evaluation

The mechanical properties of the obtained coatings were analyzed with nanoindentation tests. Nanoindentation measurements were carried out using the iMicro™ from Nanomechanics, Inc, nanoindenter to evaluate the hardness.

Indentations were performed using a diamond Berkovich tip with a constant depth of  $d = 500$  nm and a strain rate of 0.2 1/s. Test parameters were kept fixed for all the samples.

Indentations were spaced sufficiently far apart so that the indentation behavior was not affected by the presence of adjacent indentations, in accordance with the ISO standard 14577-4:2016.

A number of six indentations were performed for each sample. For sake of comparison, the magnesium substrate was also investigated.

### 2.4 | Corrosion resistance evaluation

The corrosion resistance of the coating was analyzed by potentiodynamic polarization tests, electrochemical impedance spectroscopy (EIS), and scanning vibrating electrode technique (SVET) at ambient temperature.

The potentiodynamic polarization tests were performed in a solution containing 0.1 M  $\text{Na}_2\text{SO}_4$  and 0.05 M NaCl. The solution was chosen to simulate a moderate-aggressive environment containing both sulfates and chlorides. The tests were performed with an AMEL 2549 Potentiostat, using as reference electrode a saturated calomel electrode and a platinum electrode as counter electrode with a scan rate of 0.4 mV/s. The scans were performed in a potential range from  $-2.1$  to  $-0.3$  V

evaluating the anodic and cathodic branch in a unique test. Before the test, the sample was left immersed in the electrolyte for 1 h for open circuit potential (OCP) stabilization. The tests were repeated five times. The EIS measurements were performed in the solution previously described at the value of the open circuit potential and in a frequency range between  $10^5$  and  $10^{-2}$  Hz with a perturbation amplitude of 5 mV. Before the test, the sample was left immersed for 1 h for OCP stabilization. The impedance measurements were recorded with a Materials Instrument spectrometer coupled with the 2549 Potentiostat and the ZView software was used for the fitting of impedance spectra.

SVET was applied to verify if the sealing treatment applied to the PEO coating could prevent the development of crevice corrosion on AZ80. For this purpose, the local electrochemical behavior of AZ80 coated with sealed PEO was compared to that of a PEO-coated AZ80 sample without sealing treatment. Both types of samples were mounted in an epoxy resin mold and their cross-sections were exposed by means of mechanical grinding (SiC paper up to the 2000 grade). The last grinding step (2000 grade) was carried out employing ethanol as coolant in order to avoid premature corrosion of Mg. Before the SVET analysis, the surfaces were rinsed with ethanol and then dried with compressed air.

The SVET equipment employed was the commercial Uniscan SCV370, comprising a Pt probe whose tip was  $50\ \mu\text{m}$  in diameter. The following operational parameters were used: Probe-sample distance =  $180\ \mu\text{m}$ ; vibration amplitude =  $25\ \mu\text{m}$  (peak-to-peak); scan speed =  $500\ \mu\text{m}/\text{s}$ ; step size =  $50\ \mu\text{m}$ ; and sensitivity =  $800\ \mu\text{V}$ . The scanned area was respectively equal to  $11 \times 8\ \text{mm}^2$  and  $13 \times 8\ \text{mm}^2$  for the nonsealed and sealed samples, resulting in total testing times of 90 min and 105 min, respectively. The working electrolyte employed was a near-neutral aerated 0.01 M NaCl solution (pH  $\approx 5.6$ ,

conductivity  $k \approx 1200\ \mu\text{S cm}^{-1}$ , volume  $\approx 800\ \text{ml}$ ). Only one SVET scan was executed for each ground sample, as all resulting surfaces completely corroded after 90 min of exposure to the NaCl solution. Every test was reproduced at least twice and their reproducibility was asserted. During immersion, in-situ optical micrographs were taken from the alloy surface using a Hirox 3D Digital Microscope. The same equipment was used for post-immersion analysis on dried samples.

## 3 | RESULTS AND DISCUSSION

### 3.1 | Microstructural characterization

The cross-section of the samples PEO treated with and without the sealing treatment were observed by SEM in backscattered electron mode and the results can be seen in Figure 1.

For the two samples, a good adhesion between the substrate and the coating can be observed, in fact no detachment between the substrate and the coating was found in the micrographs. In detail, the presence of a uniform oxide layer about  $20\ \mu\text{m}$  thick can be noted. It is also clear from the reported images that the pores that characterize this type of coating are sealed on the top of the coating in the sample PEO+sealing (Figure 1b). The porosity, however, seems to be closed by the sealing treatment but it is always observable on the cross-section in the coating thickness, indicating that the sealing process does not modify the microstructure of the coating. Also, energy dispersive X-ray spectroscopy (EDS) analysis was performed on the coatings in the two samples and the results are reported in Table 1. The coating is mainly composed of magnesium oxide with also the presence of silicates and phosphates in accordance with the composition of the substrate and of the electrolyte. No significant changes in the elemental

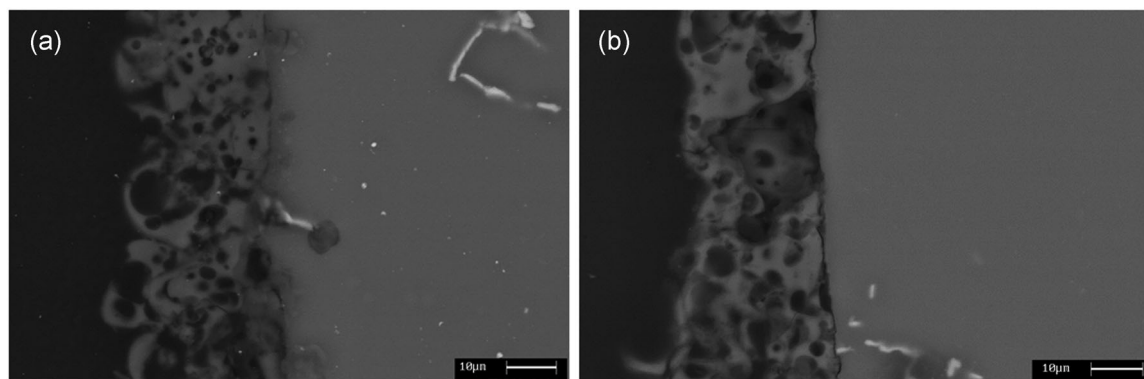


**FIGURE 1** Scanning electron microscope (SEM) micrographs of the cross-section of the plasma electrolytic oxidation (PEO)-treated (a) and PEO+sealing (b) samples

**TABLE 1** Results of energy dispersive X-ray spectroscopy semi-quantitative results (wt%) performed on the cross-section of the sample PEO and PEO+sealing

	Mg %	Si %	O %	P %	Al %	Na %
PEO	24.0	12.4	38.7	11.9	3.0	10.0
PEO+sealing	25.2	11.4	44.8	8.4	2.5	7.7

Abbreviation: PEO, plasma electrolytic oxidation

composition can be observed after the sealing treatment, as predictable due to the fact that this process is performed in distilled water.

In order to identify the different phases obtained in the PEO coatings, X-ray diffraction (XRD) analyses were also performed and the spectra are reported in Figure 2.

XRD analyses confirmed the results of EDS with no significant differences between the samples with and without the sealing treatment. From the reported data, the coating is mainly composed of magnesium oxide with also the presence of magnesium silicate and phosphate. This fact is due to the particular mechanism of formation of PEO coatings that permit the formation not only of the substrate oxide but also of compounds coming from the electrolyte.<sup>[13]</sup> In this case, sodium silicates and phosphate were present in the electrolyte, so the composition of the coating resulted in accordance with the one of the electrolyte and also with the ones previously reported in literature.<sup>[14–16]</sup> Mg peaks can also be found in the spectra due to the reflection from the substrate.

### 3.2 | Mechanical resistance evaluation

The mechanical properties of the PEO coatings produced on magnesium alloys were measured with nanoindentation tests. The measurements were

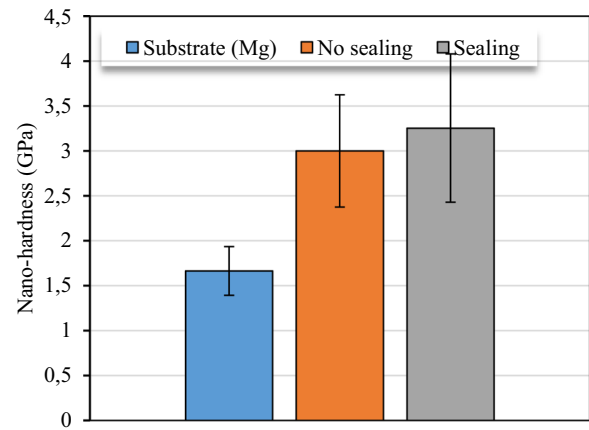


**FIGURE 3** Nano-hardness values for the untreated, PEO-treated, and PEO+sealing samples. PEO, plasma electrolytic oxidation

performed in the cross-section of the samples and the results are reported in Figure 3. The p-h curves were not recorded considering that the measurements were performed in constant depth mode. The comparison between the samples with and without the sealing treatment show that the nano-hardness is not influenced by the sealing treatment. This fact could be well explained considering that during the sealing treatment, no additives were added to the coating and so no significant modification in the mechanical resistance can be observed. Moreover, this is in accordance also with the microstructural characterization described in Section 3.1: The sealing treatment closes the pores on the top of the coating but the structure of the oxide layer remains porous in the thickness and so the mechanical properties resulted unaltered. The mechanical resistance of the obtained coatings is also in accordance with the one commonly considered for PEO-treated magnesium samples.<sup>[19–21]</sup>

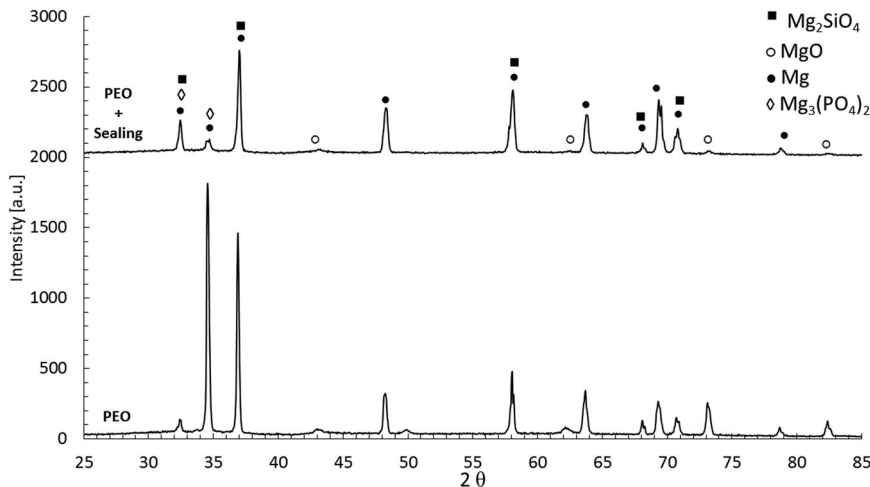


**FIGURE 2** X-ray diffraction spectra of the PEO and PEO+sealing samples. PEO, plasma electrolytic oxidation

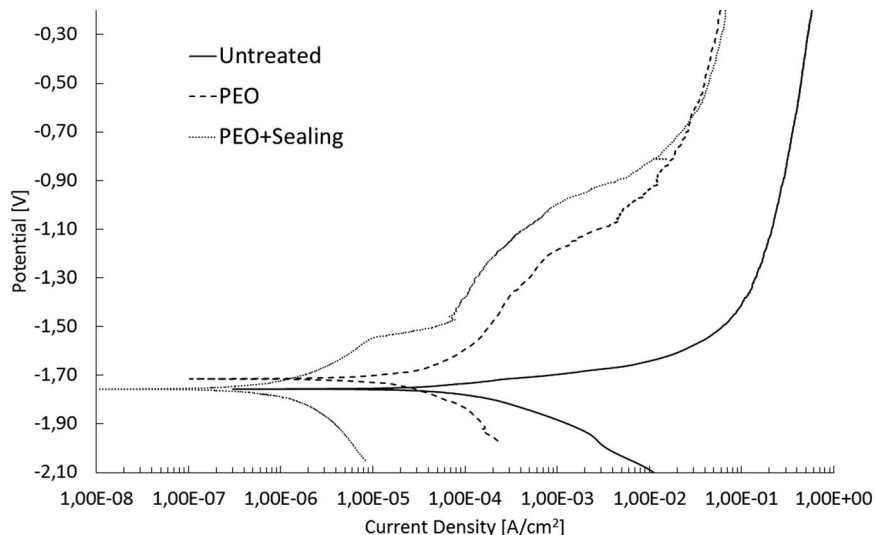


**FIGURE 4** Potentiodynamic polarization plots of the different samples recorded after 1 h of immersion (test electrolyte 0.1 M  $\text{Na}_2\text{SO}_4$ +0.05 M NaCl)

### 3.3 | Corrosion resistance evaluation

The corrosion resistance of the different samples was first of all preliminary investigated with potentiodynamic polarization tests in a solution containing both sulfates and chlorides. The results are reported in Figure 4.

From the screening with potentiodynamic polarization, remarkable differences between the different samples in term of corrosion resistance can be observed. Both the PEO-treated samples show an increase in the corrosion resistance, if compared with the untreated sample especially in term of anodic current, with a clear shift to lower anodic currents for the PEO-treated samples. In particular, the sample PEO-treated and sealed seems the best in terms of corrosion performances. No significant differences can be however found in the corrosion potential for the different samples. Considering the fact that PEO coatings are thick ceramic insulant coatings, corrosion currents cannot be calculated with the Tafel law. Considering this, in order to further

investigate the corrosion performance of the samples, EIS tests were also performed in the same solution used for the potentiodynamic polarization tests. The results in terms of Nyquist plot are reported in Figure 5. The data were also fitted with the software z-view using the circuits reported in Figure 6 that are also the typical ones used to fit PEO coatings<sup>[22–24]</sup> obtaining good fitting results. Actually, in the plots, the points represent the experimental data and the lines, the result of the fitting. In detail, for the untreated sample, a simple circuit with one parallel R-CPE (Figure 6a) was used in order to simulate the presence and the corrosion behavior of only the natural oxide layer, instead for PEO coatings, the more complex circuit with two parallel R-CPE (Figure 6b) was used in order to simulate the typical double-layer structure of PEO coatings<sup>[24]</sup> with the presence of an inner layer and an external porous layer that could be functionalized, for example, with particles addition.<sup>[25,26]</sup> The inner layer is in this case very thin

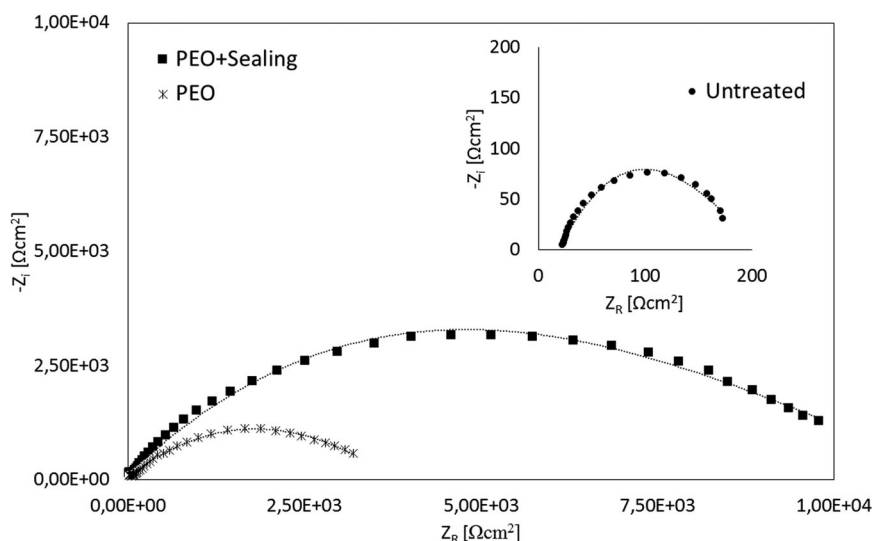


**FIGURE 5** Nyquist plots obtained from electrochemical impedance spectroscopy (EIS) tests of the different samples after 1 h of immersion (test electrolyte 0.1 M  $\text{Na}_2\text{SO}_4$ +0.05 M NaCl)

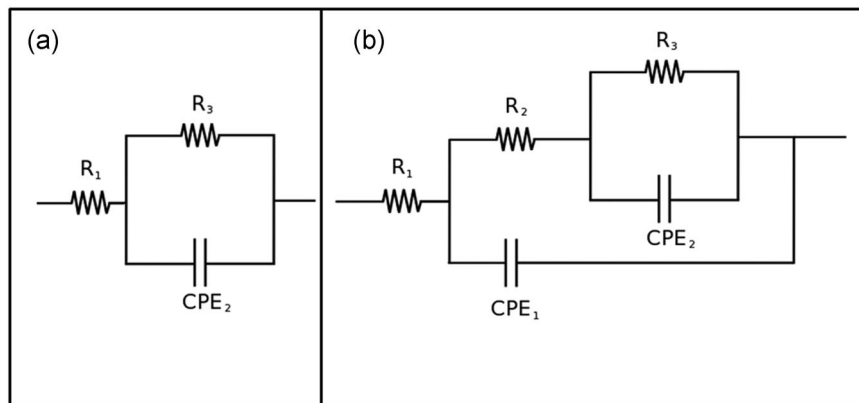


**FIGURE 6** Equivalent circuits used to fit the data coming from EIS tests. The circuit in (a) was used for the untreated sample instead the one in (b) for the PEO-treated sample. EIS, electrochemical impedance spectroscopy; PEO, plasma electrolytic oxidation

and not clearly observable in the SEM images of the cross-section but is always present in PEO coatings and is the zone near the substrate where there is a reduction in the porosity.

Considering in detail the physical meaning of the different electrical parameters:  $R_1$  represents the resistance of the solution;  $R_2$  is related to the polarization resistance of the external porous layer; and  $R_3$  represents the natural oxide layer (Figure 6a) or the inner layer of the PEO (Figure 6b). In the circuit, a constant phase element instead of a capacitance was used, since often the measured capacitance is not ideal. In this case,  $CPE_2$  is related to the porous layer, whereas  $CPE_3$  to the oxide layer (Figure 6a) or to the inner layer (Figure 6b). The results of the fitting are reported in Table 2. First of all, from the observation of the Nyquist plots, it can be observed that the EIS test confirmed the results obtained from potentiodynamic polarization. In fact, a remarkable increase in the resistance, represented by the real part of the impedance, can be observed for the PEO-treated samples if compared with the untreated one. Considering the samples with and without the sealing treatment, the resistance of the sample with the sealing is higher confirming that this treatment produces an increase in the corrosion resistance.

**TABLE 2** Results of the fitting of the experimental data coming from the potentiodynamic polarization

	Untreated	PEO	PEO+sealing
$R_1$ [ $\Omega \text{ cm}^2$ ]	23.59	25.04	27.06
$R_2$ [ $\Omega \text{ cm}^2$ ]	-	3978	8476
$R_3$ [ $\Omega \text{ cm}^2$ ]	178.70	248.62	234.93
$Q_2$ [ $\text{F Hz}^{1-n}$ ]	-	$2.97 \times 10^{-7}$	$4.99 \times 10^{-8}$
$n_2$	-	0.98	0.97
$Q_3$ [ $\text{F Hz}^{1-n}$ ]	$7.90 \times 10^{-6}$	$5.10 \times 10^{-6}$	$1.42 \times 10^{-6}$
$n_3$	0.96	0.76	0.78
$\chi^2$	0.001	0.003	0.001

Abbreviation: PEO, plasma electrolytic oxidation

From the analysis of the fitting of the experimental data reported in Table 2, an increase of more than one order of magnitude in the polarization resistance  $R$  passing from the untreated sample to the PEO-treated samples is clearly observable. Moreover, after the sealing treatment the  $R_2$  value, related to the corrosion behavior of the external layer, doubles confirming that the sealing treatment induces an increase in the corrosion resistance due to the fact that the pores resulted close on the surface after the treatment.

To further study the corrosion mechanism in the samples PEO-treated with and without the sealing treatment, SVET analyses were performed in 0.01 M NaCl (the choice of the electrolyte was performed in order to optimize the detection of the signal). It is important to note that as the propagation of filiform corrosion on AZ80 is reported under conditions of significantly higher chloride concentration,<sup>[27]</sup> FFC-like corrosion is unlikely in the present case (diluted NaCl solution). Ideally, the longitudinal section (instead of the cross-section) of the coated magnesium should be tested. However, by testing the system in such ideal configuration, in case of corrosion activities taking place underneath the coating, they would not be able to be detected by the SVET probe. Indeed, as is often the case with SVET analysis on protective coatings,<sup>[28]</sup> even with intense corrosion processes occurring at the coating/substrate interface, the assignment of the corresponding ionic fluxes is limited due to the dielectric properties of the coating. It is for that reason that SVET studies on coated-systems are generally carried out on scratched coating surfaces or on the cut edge of the system (sample cross-section). This occurred also in the present study, in fact SVET tests were performed first in the longitudinal sections, but no relevant current densities were detected over the exposed surface in both the samples analyzed. However, as evidenced by the previously reported electrochemical test, some relevant differences in the corrosion properties between the sealed and unsealed

samples were found. Therefore, in the present study, the local electrochemical monitoring of the protective properties of the PEO coatings on AZ80 was chosen to be performed on the cross-section of the systems. Indeed, at this configuration, the permeability of water exclusively in the direction perpendicular to the coating is not under test. On the other hand, it constitutes a more severe situation, in which the access of water to the substrate through the coating is much facilitated. Hence, the extent of water transport through the PEO structures can be indirectly monitored depending on the intensity of the resulting crevice corrosion process. Figure 7a presents a current density map obtained from the cross-section of an AZ80 sample presenting PEO coating without sealing. As expected for Mg alloys exposed to aqueous NaCl solution, corrosion reactions were clearly identified on the alloy surface. The anodic activity was mainly detected near the borders of the sample, while the cathodic activity was rather depicted on central regions of AZ80. The in-situ optical micrographs taken during the first 30 min of immersion (Figure 7b) revealed the rise of bubbles

related to hydrogen evolution reaction (HER). The bubbles appeared on various regions of the surface, but were preferentially located nearby the coating regions associated to the depicted anodic activity.

These results combined might constitute a classic case of crevice corrosion: the porous coating at the sample peripheries would allow the electrolyte to reach the lateral parts of AZ80, inducing the formation of a differential aeration cell. The external sample surface more exposed to oxygen would rather support oxygen reduction reaction, while anodic dissolution would preferentially occur on the lateral surfaces.

However, it is reported that crevice corrosion typically does not occur with magnesium alloys, because corrosion of Mg is relatively insensitive to oxygen concentration gradients.<sup>[29,30]</sup> For instance, the principal cathodic reaction on Mg involves the reduction of water rather than oxygen (Equation (1)).<sup>[31]</sup> Filiform corrosion (FFC) however, which is a special type of crevice corrosion, is largely associated to the corrosion of Mg and its alloys.<sup>[29–31]</sup> As explained by Williams et al,<sup>[31]</sup> the Mg

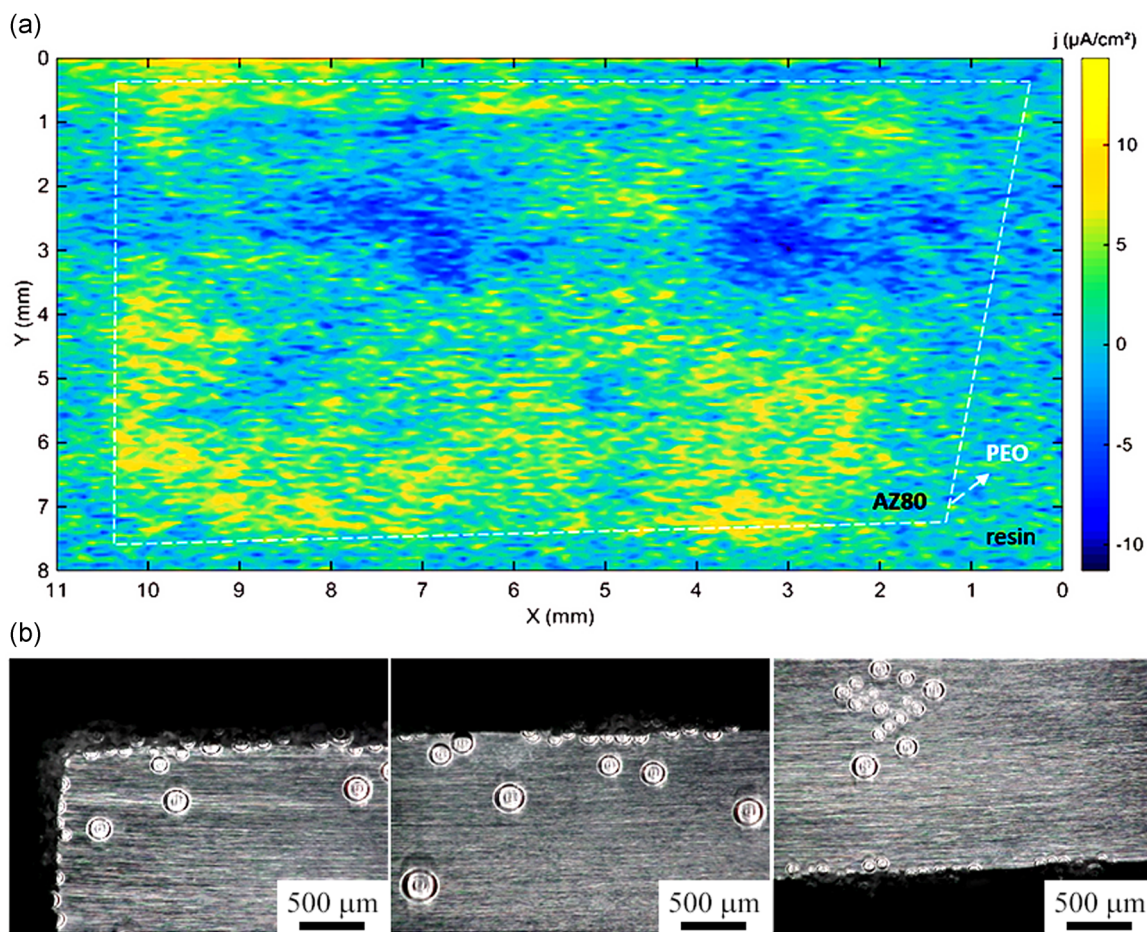
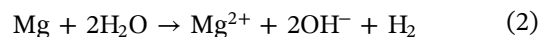
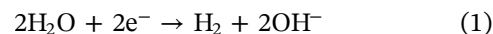


**FIGURE 7** (a) SVET current density ( $j/\text{mA cm}^{-2}$ ) map obtained from the cross-section of an AZ80 sample with nonsealed PEO coating exposed to 0.01 M NaCl solution. 90 min of immersion were necessary for completing the entire scan. (b) Corresponding optical micrographs obtained during the first 30 min of immersion

FFC propagation would be highly dependent upon both the availability and activity of water at the metal surface. Their complementary SVET investigation on AZ31<sup>[32]</sup> demonstrated that the dark dendrite-like features, which characterize FFC are built through the action of several mobile local anodes that couple to cathodically activated corroded regions left behind. In a similar way, in the present case, the anodic attack associated to the porous PEO coating would advance due to coupling with the external alloy surface directly in contact with water, increasing the rate of the overall corrosion reaction of Mg on the border regions (Equation (2)).<sup>[33]</sup> In other words, the difficult water transport through the nonsealed PEO coating could allow for the advancement of this type of crevice corrosion induced by water activity gradient. The preferential formation of hydrogen bubbles on the AZ80/coating interfaces (Figure 7b) also indicates the preferred development of cathodes on the peripheral regions of the alloy right next to the coated surfaces. It is beyond the scope of this paper to explain the mechanism of the crevice corrosion process verified on the cross-section of

the nonsealed PEO coating sample. Nonetheless, the clearly distinct corrosion behavior of sealed and unsealed coatings observed in the presented SVET analysis could not be ignored.



It is worth noting that dark corrosion products likely enriched in noble Al–Mn particles—typically accredited as the source for the cathodic activation<sup>[31]</sup>—were not observed in this short term test. The few bubbles detected on the center of the alloy (whose positions appeared coincident to the spots presenting cathodic activity; Figure 7b) probably arose from HER taking place on Al–Mn cathodic particles.<sup>[34]</sup>

Figure 8 presents a current density map obtained from the cross-section of an AZ80 sample coated with sealed PEO exposed to 0.01 M NaCl solution. Once again,

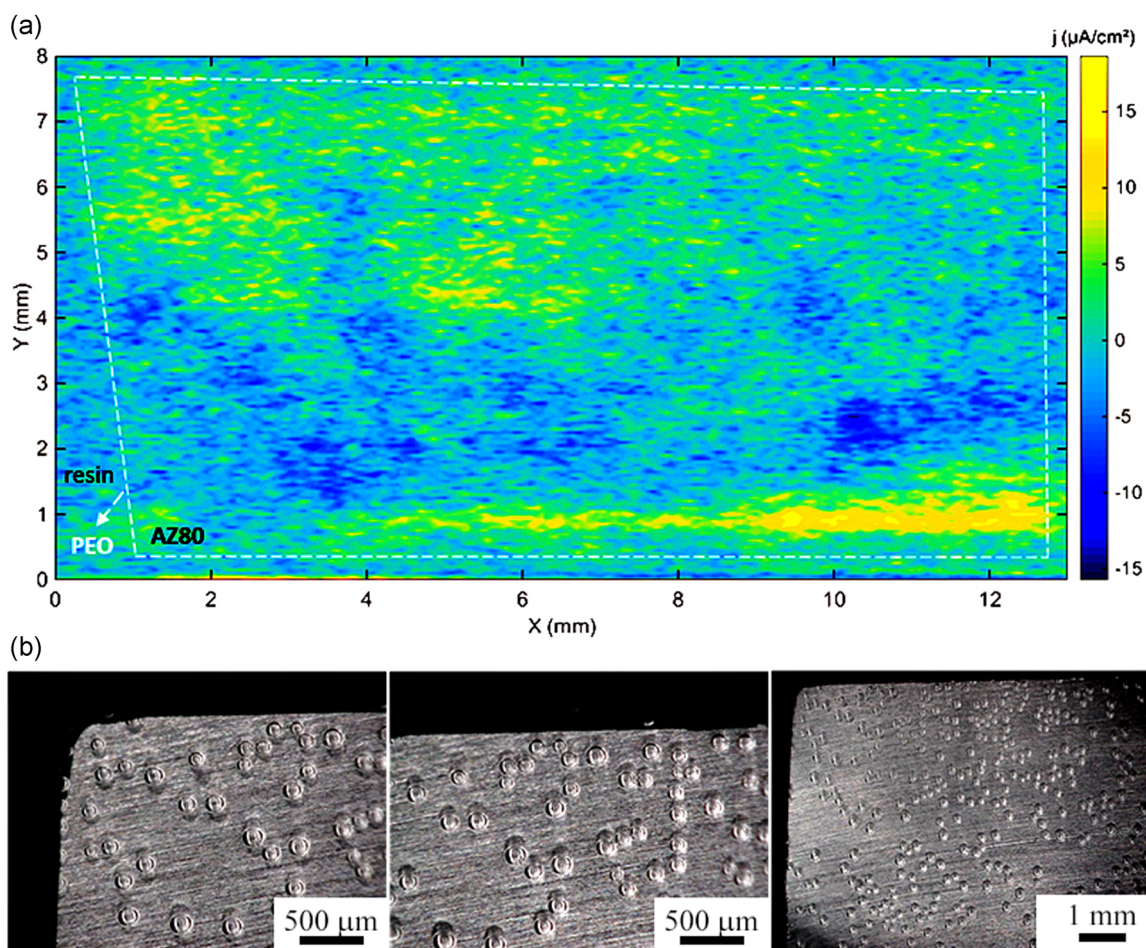


**FIGURE 8** (a) SVET current density ( $j/\text{mA cm}^{-2}$ ) map obtained from the cross-section of an AZ80 sample with sealed PEO coating exposed to 0.01 M NaCl solution. For completing the entire scan, 105 min of immersion was necessary. (b) Corresponding optical micrographs obtained during the first 30 min of immersion

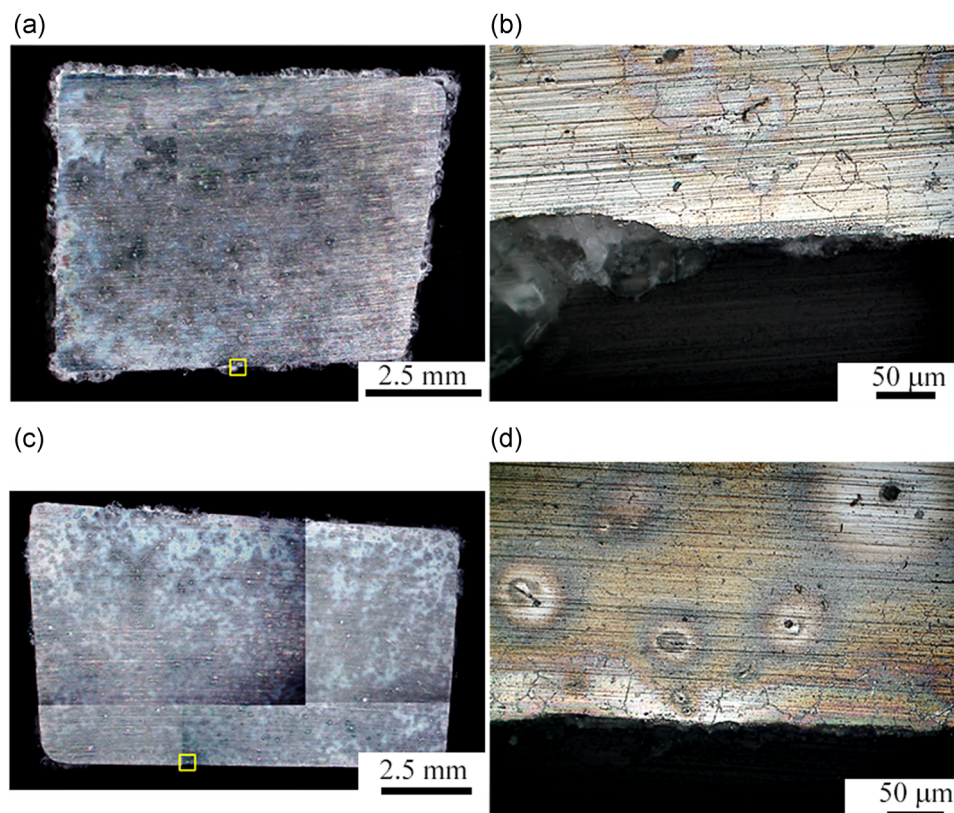


**FIGURE 9** Optical micrographs from the cross-sections of the AZ80 samples with: (a,b) Nonsealed and (c,d) sealed PEO coatings respectively after 90 and 105 min of immersion in 0.01 M NaCl. (b) and (d) insets of higher magnification from the regions indicated in (a) and (c), respectively

corrosion activity was clearly attributed to the alloy surface. However, in this case, anodic reactions did not take place preferentially on the border regions. Instead, both anodic and cathodic processes appeared rather homogeneously distributed throughout the AZ80 surface. This finding indicates that crevice corrosion was less likely to occur on the alloy with sealed PEO coating. This notion was reinforced by the in-situ optical microscopy analysis, which revealed a homogeneous generation of bubbles all around the AZ80 surface (Figure 8b).

Postimmersion optical micrographs revealed the presence of quite porous white corrosion products (probably  $\text{Mg}(\text{OH})_2$ <sup>[35]</sup>) for the two AZ80/PEO coating systems investigated (Figure 9). However, for the nonsealed coating, the precipitates were mainly detected on the borders, directly over the coating referred regions (Figure 9a,b). On the contrary, in the case of the sealed PEO coating, corrosion products were much less present on the borders and seemed rather homogeneously distributed on the surface (Figure 9c,d). For the latter, corrosion also manifested in the form of pit-like features. For instance, corrosion of magnesium alloys in chloride media is considered to typically initiate as irregular pits, which spread laterally and cover the whole surface.<sup>[29]</sup> Williams et al<sup>[31]</sup> reported

the development of “pin-holes” on the film-covered Mg surface exposed to neutral NaCl solution and were referred as previous sites of HER and bubbling in the beginning of immersion.

## 4 | CONCLUSIONS

The mechanical properties and the corrosion resistance of PEO-coated AZ80 magnesium alloy were evaluated before and after a sealing treatment in boiling water. The nano-hardness values resulted the same for both the samples, whereas the corrosion resistance was strongly influenced by the sealing treatment. In fact, the sealed sample was remarkably more resistant than the unsealed one. Moreover, the SVET tests revealed that in the sample without the sealing treatment, the corrosion proceeded along the cross-section, with a mechanism of crevice corrosion. This type of corrosion was induced by the water activity gradient, due to difficult water transport through the nonsealed PEO coating. After the sealing treatment, both anodic and cathodic processes appeared homogeneously distributed on the surface indicating that crevice corrosion was less likely to occur after the sealing treatment.

## ORCID

Luca Pezzato  <http://orcid.org/0000-0001-5016-8790>

## REFERENCES

- [1] E. Aghion, B. Bronfin, D. Eliezer, *J. Mater. Process Technol.* **2001**, *117*, 381.
- [2] G. L. Makar, *J. Electrochem. Soc.* **1990**, *137*, 414.
- [3] B. V. Vladimirov, B. L. Krit, N. V. Morozova, A. V. Epel'feld, *Surf. Eng. Appl. Electrochem.* **2014**, *50*, 514.
- [4] J. Zhang, C. Wu, *Recent Pat. Corros. Sci.* **2010**, *2*, 55.
- [5] M. F. Montemor, A. M. Simões, M. G. S. Ferreira, M. J. Carmezim, *Appl. Surf. Sci.* **2008**, *254*, 1806.
- [6] X. B. Chen, N. Birbilis, T. B. Abbott, *Corrosion* **2011**, *67*, 035005.
- [7] C. Blawert, W. Dietzel, E. Ghali, G. Song, *Adv. Eng. Mat.* **2006**, *8*, 511.
- [8] Z. Rajabalizadeh, D. Seifzadeh, A. Habibi-Yangjeh, T. Mesri Gundoshmian, S. Nezamdoust, *Surf. Coat. Technol.* **2018**, *346*, 29.
- [9] X. Li, X. Wang, W. Shi, H. Liu, H. Yu, *Modern Surf. Eng. Treat.* **2013**, *4*, 75.
- [10] T. W. Clyne, S. C. Troughton, *Int. Mat. Rev.* **2018**, *64*, 127.
- [11] L. Pezzato, K. Brunelli, S. Gross, M. Magrini, M. Dabalà, *J. Appl. Electrochem.* **2014**, *44*, 867.
- [12] E. Matykina, R. Arrabal, P. Skeldon, G. Thompson, *Surf. Coat. Technol.* **2009**, *54*, 6767.
- [13] C. Blawert, P. Bala Srinivasan, in *Surface Engineering of Light Alloys: Aluminium, Magnesium and Titanium Alloys* H. Dong (Ed: ), Woodhead Publishing, Oxford **2010**.
- [14] L. Pezzato, V. Angelini, K. Brunelli, C. Martini, M. Dabalà, *Transact. Nonferrous Met. Soc. China* **2018**, *28*, 193.
- [15] M. Mohedano, C. Blawert, M. L. Zheludkevich, *Surf. Coat. Technol.* **2015**, *269*, 145.
- [16] Luca Pezzato, Katya Brunelli, Riccardo Babbolin, Paolo Dolcet, Manuele Dabalà, *Int. J. Corr.* **2017**, *2017*
- [17] M. Serdechnova, M. Mohedano, B. Kuznetsov, C. L. Mendis, M. Starykevich, S. Karpushenkov, J. Tedim, M. G. S. Ferreira, C. Blawert, M. L. Zheludkevich, *J. Electrochem. Soc.* **2017**, *164*, C36.
- [18] N. Hu, X. Dong, X. He, J. F. Browning, D. W. Schaefer, *Corr. Sci.* **2015**, *97*, 17.
- [19] A. Dey, R. Umarani, H. K. Thota, P. Bandyopadhyay, A. Rajendra, A. K. Sharma, A. K. Mukhopadhyay, *Surf. Eng.* **2014**, *30*, 913.
- [20] L. White, S. Neralla, R. Kotoka, Y. Jang, Y. Yun, J. Sankar, Presented at ASME, 2013 International Mechanical Engineering Congress and Exposition IMECE2013, San Diego, California, USA, 2013.
- [21] X. Wu, P. Su, Z. jiang, S. Meng, *Appl. Mater. Interface* **2010**, *2*, 808.
- [22] D. Sreekanth, N. Rameshbabu, K. Venkateswarlu, *Ceram. Int.* **2012**, *38*, 607.
- [23] L. Pezzato, K. Brunelli, P. Dolcet, M. Dabalà, *Surf. Coat. Technol.* **2016**, *307*, 73.
- [24] R. Arrabal, E. Matykina, T. Hashimoto, P. Skeldon, G. E. Thompson, *Surf. Coat. Technol.* **2009**, *3*, 2207.
- [25] P. Cerchier, L. Pezzato, K. Brunelli, P. Dolcet, A. Bartolozzi, R. Bertani, M. Dabalà, *Mater. Sci. Eng.: C* **2017**, *75*, 554.
- [26] L. Pezzato, P. Cerchier, K. Brunelli, A. Bartolozzi, R. Bertani, M. Dabalà, *Surf. Eng.* **2018**, *35*, 325.
- [27] C. Liu, Y. Xin, G. Tang, P. K. Chu, *Mater. Sci. Eng.: A* **2007**, *456*, 350.
- [28] A. C. Bastos, M. C. Quevedo, O. V. Karavai, M. G. S. Ferreira, *J. Electrochem. Soc.* **2017**, *164*, C973.
- [29] T. L. S. L. Wijesinghe, D. J. Blackwood, *Corr. Sci.* **2008**, *50*, 23.
- [30] G. L. Makar, J. Kruger, *Int. Mater. Rev.* **1993**, *38*, 138.
- [31] G. Williams, R. Grace, *Electrochim. Acta* **2011**, *56*, 1894.
- [32] G. Williams, H. Ap llwyd dafydd, R. Grace, *Electrochim. Acta* **2013**, *109*, 489.
- [33] G. Song, *Adv. Eng. Mater.* **2005**, *7*, 563.
- [34] Y. Yang, F. Scenini, M. Curioni, *Electrochim. Acta* **2016**, *198*, 174.
- [35] M. C. Merino, A. Pardo, R. Arrabal, S. Merino, P. Casajús, M. Mohedano, *Corros. Sci.* **2010**, *52*, 1696.

**How to cite this article:** Pezzato L, Coelho LB, Bertolini R, et al. Corrosion and mechanical properties of plasma electrolytic oxidation-coated AZ80 magnesium alloy. *Materials and Corrosion*. 2019;1–10. <https://doi.org/10.1002/maco.201910847>